Chain Segmental Motion and Side-Chain Internal Rotations of Poly(1-naphthylalkyl acrylate)s in Solution Studied by ^{13}C Nuclear Magnetic Relaxation

A. Spyros and Photis Dais*

Department of Chemistry, University of Crete, 71409 Iraklion Crete, Greece

Frank Heatley*

Department of Chemistry, University of Manchester, Manchester M13 9PL, U.K.

Received March 22, 1994®

ABSTRACT: ^{13}C longitudinal relaxation times and nuclear Overhauser enhancements were measured as a function of temperature in three magnetic fields for a series of poly(1-naphthylalkyl acrylate)s in 1,1,2,2-tetrachloroethane-d_2. Variable-temperature ^{13}C transverse relaxation time measurements at 75.4 and 125.7 MHz also were undertaken. The relaxation data have been described by using various models for main-chain segmental motion and side-chain internal rotations. Among these, the Dejean–Laupretre–Monnerie (DLM) model offered the best description of segmental motion for the poly(1-naphthylalkyl acrylate) chains. Internal rotations about the side-chain bonds, including naphthyl internal motion, were described by hindered rotations superimposed on segmental motions, the latter being described by the DLM model. An attempt was made to correlate rates and activation energies associated with the various modes of reorientation in the aforementioned polymers with the rates of excimer formation between the side-chain naphthalene chromophores.

Introduction

Emission spectra and photophysical processes in polymers containing pendant aromatic groups have been investigated extensively in the last decade.[1,2] In particular, the energy transfer between pendant naphthalene chromophores can result in excimer formation, unusually efficient quenching by small molecules, and energy transfer to chemically bound traps. These energy-transfer processes in synthetic polymers appear to mimic similar effects in plant photosynthesis and to have practical consequences in the photodegradation and/or photostabilization of commercial polymers. A detailed interpretation of photophysical results requires, among other factors, a knowledge of the stereochemical composition and the chain dynamics of the polymer system.[3–5] The first factor determines the effective "concentration" of the pendant chromophores on the polymer chain for efficient intrachain energy transfer. The second factor controls the sandwiched parallel disposition of two pendant chromophores and the formation of excimer through the chain segmental diffusion and internal rotation about bonds of the side chains.

To investigate the effect of segmental motion and internal rotation as well as that of tacticity[6] on the intramolecular excimer formation, the dynamics of a series of naphthalene-containing polymers have been examined by the ^{13}C nuclear magnetic relaxation technique. These polymer systems, poly(1-naphthyl acrylate) (PNA), poly(1-naphthylmethyl acrylate) (PNMA), and poly[2-(1-naphthyl)ethyl acrylate] (PNEA) constitute a series in which the naphthalene chromophore is located progressively further from the main chain. The dynamics of the first member of the series have been reported earlier.[7] In this study, additional experimental data for PNA are presented and analyzed on the basis of theoretical dynamic models.

The emission characteristics of these polymers are discussed as well in relation to the dynamics and microstructure of the polymer chain.

* Abstract published in *Advance ACS Abstracts*, July 15, 1994.

Experimental Section

The synthesis of the monomers used to obtain the polymers and the polymerization procedure have been described in detail in an earlier publication.[6]

NMR Measurements. ^{13}C NMR relaxation measurements were conducted at ^{13}C Larmor frequencies of 125.7, 100.5, 75.4, and 62.5 MHz on a Varian Unity 500, Bruker WH400, Varian XL-300, and Bruker AM250 spectrometers, respectively, under broadband proton decoupling. The sample temperature was controlled to within ±1 °C by means of precalibrated thermocouples in the probe inserts.

The longitudinal relaxation times (T_1) were measured by the standard IRFT method with a repetition time longer than $5T_1$. A total of 128–500 acquisitions were accumulated, depending on the polymer and the spectrometer used, for a set of 11–15 "arrayed" τ values. Values of T_1 were determined by a three-parameter nonlinear procedure with a rms error of ±10% or better. ^{13}C NOE experiments were carried out by inverse gated decoupling, at least two experiments being performed for each temperature value. Delays of at least 10 times the longest T_1 were used between 90° pulses. NOE values are estimated to be accurate within ±15%. Measurements of ^{13}C spin–spin relaxation times (T_2) were performed by using the Carr–Purcell–Meiboom–Gill[8] (CPMG) pulse sequence. However, to avoid an irreversible diminution in the measured T_2 values as compared to the true values,[9] proton decoupling was switched off during echo formation, but reestablished during acquisition and over a long delay time ($\sim 5T_1$) before the repetition of the pulse sequence. The accuracy of the measured T_2 values is estimated to be ±15–20%.

Samples of PNA, PNMA, and PNEA in deuterio-1,1,2,2-tetrachloroethane (TCE-d_2) (10% w/v) were degassed by several freeze–pump–thaw cycles and sealed in 5-mm NMR tubes. Nevertheless, measurements with undegassed samples did not show any measurable change in the ^{13}C relaxation parameters relative to those of the degassed samples.

Viscosity measurements were performed using Ubbelohde type dilution viscometer at 30 °C. For PNMA and PNEA solutions in TCE-d_2, the intrinsic viscosities, $[\eta]$, and Huggins' constants, k', in eq 1, were found to be 0.2127, 2.084 and 0.2425, 1.124, respectively.

$$\eta_{sp}/C = [\eta] + k'[\eta]^2 C \qquad (1)$$

Numerical Calculations. The relaxation data were analyzed by using the MOLDYN program,[10] modified to include the spectral density functions of the various models used in the

0024-9297/94/2227-5845$04.50/0

present study. Details of the program and the fitting procedure by employing various models for the backbone and side-chain motions have been given elsewhere.[10-12] The relaxation parameters for the CH_2 group were not included in the optimization procedure in most cases. This resonance was broadened so much by the effect of tacticity that its relaxation parameters were difficult to measure accurately. However, in order to examine the effect of the librational motion of the backbone C–H vectors and, hence, the existence of different local dynamics along the main chain, the relaxation data of the CH_2 group of PNA at 125.7 MHz were used in the present analysis. The splitting of this peak was not severe relative to that in the corresponding peaks of the other two polymers,[6] and the sensitivity was superior to that obtained at 50.3 and 75.4 MHz.[7] The measured T_1 values of this carbon resonance are estimated to be accurate within ±15%.

Relaxation Equations. The relaxation equations used in the present fitting procedure were derived[13] on the basis of the relaxation mechanism that dominates the measured relaxation parameter. Assuming a purely ^{13}C–^{1}H dipolar relaxation mechanism,[14] the T_1, T_2, and NOE parameters can be expressed in terms of the spectral density function, $J(\omega)$, as follows (in the SI system[15]):

$$\frac{1}{T_1} = \frac{\Omega}{10}[J(\omega_H-\omega_C) + 3J(\omega_C) + 6J(\omega_H+\omega_C)] \quad (2)$$

$$\frac{1}{T_2} = \frac{\Omega}{20}[4J(0) + J(\omega_H-\omega_C) + 3J(\omega_C) + 6J(\omega_H) + 6J(\omega_H+\omega_C)] \quad (3)$$

$$\mathrm{NOE} = 1 + \frac{\gamma_H}{\gamma_C}\left[\frac{6J(\omega_H+\omega_C) - J(\omega_H-\omega_C)}{J(\omega_H-\omega_C) + 3J(\omega_C) + 6J(\omega_H+\omega_C)}\right] \quad (4)$$

and

$$\Omega = N\left(\frac{\mu_0\gamma_H\gamma_C\hbar}{8\pi^2 r_{CH}^3}\right)^2$$

where γ_H and γ_C are the gyromagnetic ratios of proton and carbon nuclei respectively, ω_H and ω_C are their Larmor frequencies, μ_0 is the vacuum magnetic permeability, $\hbar = h/2\pi$ is Planck's constant, N is the number of directly bonded protons, and r_{CH} is the C–H internuclear distance. $J(\omega)$ is related to the normalized time-correlation function (TCF), $G(t)$, that embodies all the information about mechanisms and rates of motions

$$J(\omega) = \frac{1}{2}\int_{-\infty}^{+\infty} G(t)e^{i\omega t}\,dt \quad (5)$$

The interpretation of the relaxation data by using eqs 2–4 requires one to fix or obtain from other sources the C–H bond length. No experimental value for the backbone C–H bond length of the three polymers exists in the literature, nor for the related poly(methyl acrylate) and poly(methyl methacrylate). We have used[16] r_{CH} = 1.09 A, for the backbone and side-chain C–H bond length, and 1.08 A, for the naphthyl C–H bond.

The mechanism of chemical shift anisotropy (CSA) contributes to the relaxation of the aromatic carbons of the naphthyl moiety at high magnetic fields. This relaxation contribution can be included in eqs 2 and 3 leading to[13,17]

$$\frac{1}{T_i^{obs}} = \frac{1}{T_i^{DD}} + \frac{1}{T_i^{CSA}} \quad (i = 1, 2) \quad (6)$$

where T_1^{DD} and T_2^{DD} are the dipole–dipole contributions as in eqs 2 and 3, and T_1^{CSA} and T_2^{CSA} are contributions from the chemical shift anisotropy mechanism. If the chemical shift tensor is axially symmetric, T_1^{CSA} and T_2^{CSA} are given by[13,17]

$$\frac{1}{T_1^{CSA}} = (^2/_{15})\omega_C^2\Delta\sigma^2 J(\omega_C) \quad (7)$$

$$\frac{1}{T_2^{CSA}} = (^1/_{45})\omega_C^2\Delta\sigma^2[4J(0) + 3J(\omega_C)] \quad (8)$$

where,

$$\Delta\sigma = \sigma_{33} - {}^1/_2(\sigma_{11} + \sigma_{22})$$

The NOE is given by

$$\mathrm{NOE} = 1 + \frac{\gamma_H}{\gamma_C} \times \left[\frac{\Omega[6J(\omega_H+\omega_C) - J(\omega_H-\omega_C)]}{\Omega[J(\omega_H-\omega_C) + 3J(\omega_C) + 6J(\omega_H+\omega_C)] + [(^2/_{15})\omega_C^2\Delta\sigma^2 J(\omega_C)]}\right] \quad (9)$$

The use of eqs 7–9 is an approximation, since the chemical shift tensor of the protonated carbons of the naphthyl group is not axially symmetric, as has been shown experimentally for naphthalene in the solid.[18] Nevertheless in the latter molecule, the low field major components of the tensors are directed approximately along the C–H bonds,[18] indicating that one of the vectors whose motion leads to CSA relaxation is nearly parallel to the aromatic C–H bond. In the present calculations, we have ignored higher order effects and fit our data to eqs 7–9 with an average $\Delta\sigma$ = 167 ppm value obtained from the principal values of the ^{13}C shift tensor of the protonated carbons of naphthalene.[18]

Models

Segmental Motion. A variety of models exists in the literature[19,20] describing local chain dynamics of flexible polymers in solution, in terms of a distribution of correlation times, conformational jumps, crankshaft type motions, or librational motions. An important feature of all models is the incorporation of longer correlation times to account for the observation of reduced NOE values and broad linewidths at low temperatures. Among these, models developed by Jones–Stockmayer[21] (JS), Hall–Weber–Helfand[22] (HWH), and Dejean–Laupretre–Monnerie[23] (DLM) have been used extensively to interpret the relaxation data in solution.[7,12,19,20] The JS model originates from the general "tetrahedral or diamond lattice" model first proposed by Valeur and co-workers[24] (VGJM model), and describes backbone rearrangement as a three-bond jump of the crankshaft type. The time scale of segmental motion is described by a harmonic mean correlation time, τ_h, and the breadth of the distribution of correlation times is characterized by the number of bonds, m, involved in the cooperative motion, or the quantity, $2m - 1$, which stands for the chain segment expressed in bonds that are coupled to the central three bonds. No correlated motions are assumed outside the segment of $2m - 1$ bonds. The spectral density function of the JS model is given explicitly elsewhere.[7,21]

The HWH model takes into account correlated pair transitions and isolated transitions occurring with correlation times τ_1 and τ_0, respectively. The pair transitions ensure the propagation of motion along the chain, while isolated, i.e. single-bond transitions, are responsible for damping. The HWH spectral density function is given explicitly in ref 12.

While the HWH model represented a significant advance in describing polymer chain local motions, in many cases it was found to underestimate the value of NT_1 at the minimum of the NT_1 vs $1/T$ (K^{-1}) curve. Furthermore, it could not account for different local dynamics observed at different carbon sites of a polymer chain.[12,25] The DLM model, which is a modification of the HWH model, corrects for these deficiencies by introducing an additional inde-

pendent motion. This motion is superimposed on backbone rearrangement, as described by the HWH model, and has been attributed to molecular librations of the C–H vector of limited extent inside a cone of half-angle θ, the axis of which is the rest position of the C–H bond with correlation time τ_2. Combining these two models, the composite DLM spectral density function under the condition $\tau_2 \ll \tau_0, \tau_1$ is[23]

$$J_i(\omega_i) = (1 - A)\,\mathrm{Re}\left[\frac{1}{(\alpha + i\beta)^{1/2}}\right] + A\left[\frac{\tau_2}{1 + \omega_i^2\tau_2^2}\right] \quad (10)$$

where

$$\alpha = \tau_0^{-2} + 2(\tau_1^{-1}\tau_0^{-1}) - \omega_i^2$$
$$\beta = -2\omega_i(\tau_0^{-1} + \tau_1^{-1}) \qquad 1 - A = \left[\frac{\cos\theta - \cos^3\theta}{2(1 - \cos\theta)}\right]^2 \quad (11)$$

The first term in eq 10 represents the spectral density function of the HWH model multiplied by the angular factor $(1 - A)$.

Side-Chain Motion. Composite spectral density functions for side-chain motions superimposed on the polymer backbone motion have been developed[26] recently in an attempt to describe multiple internal rotations of hydrocarbon side chains attached to the polymer backbone. Frequency-dependent ^{13}C relaxation data are described by models involving restricted multiple internal rotations. Conformational constraints imposed by the environment of the side chain are assumed to restrict the motion about certain C–C bonds to amplitudes smaller than 360°. The composite spectral density function for side-chain restricted rotations superimposed on chain segmental motion, the latter being described by the HWH model, is given by[26]

$$J(\omega) = Q \times \mathrm{Re}\left[\frac{1}{(\alpha' + i\beta')^{1/2}}\right] \quad (12)$$

where

$$\alpha' = \tau_{01}^{-2} + 2(\tau_{01}\tau_1)^{-1} - \omega_i^2 \qquad \beta' = -2\omega_i(\tau_{01}^{-1} + \tau_1^{-1})$$
$$\tau_{01}^{-1} = \tau_0^{-1} + \left(\frac{n_1\pi}{2\varphi_1}\right)^2 D_1 + \left(\frac{n_2\pi}{2\varphi_2}\right)^2 D_2 + \ldots + \left(\frac{n_n\pi}{2\varphi_n}\right)^2 D_n$$

D_i is the diffusion constant for rotation about the ith diffusion axis and φ_i is the range of angular restriction. Q is given by[26]

$$Q = \sum_{n_1,n_2,\ldots,n_n} \sum_{b_1',b_2',\ldots b_n} \times$$
$$\Gamma_{b_1b_1'n_1}(\varphi_1) d_{b_1b_2}^{(2)}(\beta_{12}) d_{b_1b_2'}^{(2)}(\beta_{12}) \cos[(b_1 - b_1')a_{12}] \times$$
$$\Gamma_{b_2b_2'n_2}(\varphi_2) d_{b_2b_3}^{(2)}(\beta_{23}) d_{b_2'b_3'}^{(2)}(\beta_{23}) \cos[(b_2 - b_2')a_{23}] \times$$
$$\ldots \times \Gamma_{b_nb_n'n_n}(\varphi_n) d_{b_nb_0}^{(2)}(\beta_{nF}) d_{nm_0}^{(2)}(\beta_{nF}) \quad (13)$$

The functions $\Gamma_{b_ib_i'n_i}(\varphi_i)$ are given explicitly in ref 27. The functions, $d_{ij}^{(2)}(\beta_{ij})$, are elements of the reduced Wigner rotation matrices,[28] which are functions of the angles β_{ij} formed between successive internal rotation axes. For tetrahedral arrangement of a hydrocarbon chain, these angles are all equal to 70.5°. The last angle β_{nF} is the angle between the nth rotation axis and the last C–H bond, and is taken as 70.5°. The indices of the first summation in eq 13 run from 0 to infinity, whereas those of the second summation run from −2 to +2. However, it should be noted that the first summation converges very rapidly, usually after 5–6 iterations. The angles a_{ij} specify the torsional angles between C_{i-2}–C_{i-1} and C_i–C_{i+1} bonds when viewed along the C_{i-1}–C_i bond axis and are all 180° for the all trans configuration of the chain. Similarly a_{iF} is the dihedral angle between the C_{i-1}–C_{i-2} and C_i–H bonds viewed along the C_{i-1}–C_i bond and takes values of ±60°. As one proceeds away from the polymer backbone, the torsional angle α_{ij} becomes meaningless, if internal rotations are assumed to be independent. This results in averaging of the torsional angle α_{nF}, which does not appear in the calculations. Moreover, the angle α_{12} does not appear in eq 13, inasmuch as segmental motion is considered isotropic. If one or more internal motions are free and the remaining rotations are restricted, eq 13 can be modified accordingly.

The effect of angular amplitude on NT_1, NT_2, and NOE is illustrated in Figure 1. NT_1 and NOE parameters increase monotonically with increasing amplitude of restricted internal rotations and reach a plateau at ca. 90°. This monotonic increase is more pronounced for faster internal motions than the backbone segmental motion, whereas comparable rates of motions lead to a smoother increase in the relaxation parameters. However, for very slow segmental motion ($\tau_1 > 10^{-7}$ s), NT_1 increases for small angular amplitudes, reaches a maximum and then decreases with increasing angle φ_i. The same complex behavior is observed[26] for the NOE values when segmental diffusion is characterized by very long correlation times.

For NT_2, for motions in the extreme narrowing region, the dependence on φ_i is qualitatively similar to that of NT_1. However, for very long correlation times ($\tau_1 > 10^{-7}$ s) of segmental motion and fast internal motions, no minimum in the NT_2 curve is observed (Figure 1). Clearly, this behavior makes NT_2 values a more reliable interpretive tool for motions described by the parameters used in the numerical calculations. Nevertheless, it should be noted that for most cases of polymers in solution, rotational correlation times for segmental motions are in the range of nanoseconds where monotonic behavior in all relaxation parameters is expected.

Internal motion, such as naphthyl internal rotation, may be added as an independent motion in the form of an appropriate stochastic process or jumps among energy minima in the potential energy curve.[29,30] Composite spectral density functions of this form have been derived[30,31] and applied successfully in the interpretation of the nuclear and dielectric relaxation data of polystyrene.[30] However, attempts to interpret the ^{13}C relaxation data of the naphthyl group in PNA using either a stochastic diffusion process or jumps in a 2-fold potential barrier were unsuccessful.[7] Therefore, a restricted rotation model developed by Gronski[32] had been adopted[7] to describe the naphthyl internal motion in PNA. Nevertheless, it is difficult to use Gronski's theory in the case of multiple internal rotations, as required by the present polymer systems. Additionally, numerical calculations proved Gronski's model to be equivalent to the description offered by eq 13 for a single restricted internal rotation. Therefore, naphthyl group internal rotation was described by means of the general spectral density function of eq 13, using $\beta_{nF} = 60°$.

Results

^{13}C Relaxation Data of Poly(1-naphthylalkyl acrylate)s. Tables 1–3 summarize the ^{13}C NT_1 and NOE factors for the methine backbone carbon, the side-chain methylene carbons, and the protonated naphthyl carbons of PNA, PNMA, and PNEA, respectively, as a function

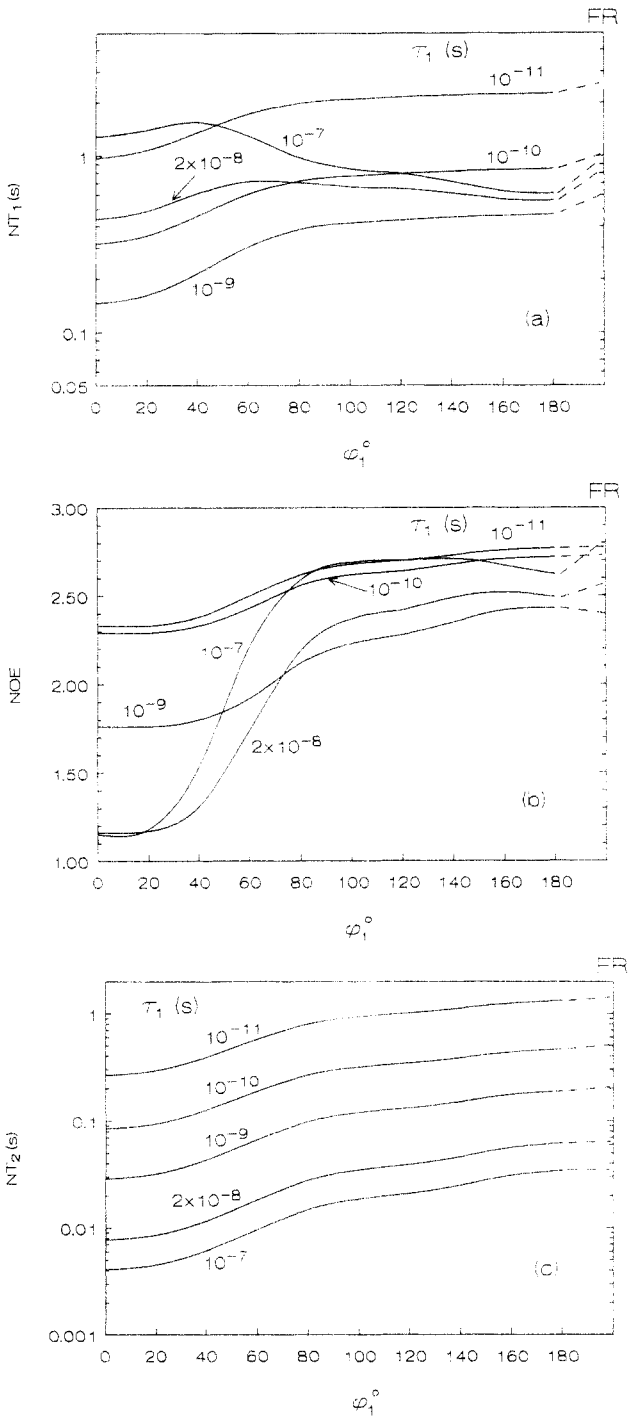

Figure 1. Spin–lattice relaxation time (NT_1), spin–spin relaxation time (NT_2), and NOE plotted as a function of φ for the first restricted rotation about the first bond and τ_1. $\tau_0 = 1.0 \times 10^{-7}$ s; $D_1 = 1.0 \times 10^{10}$ s^{-1}. FR values correspond to free internal rotation model. Calculations are at 67.905 MHz.

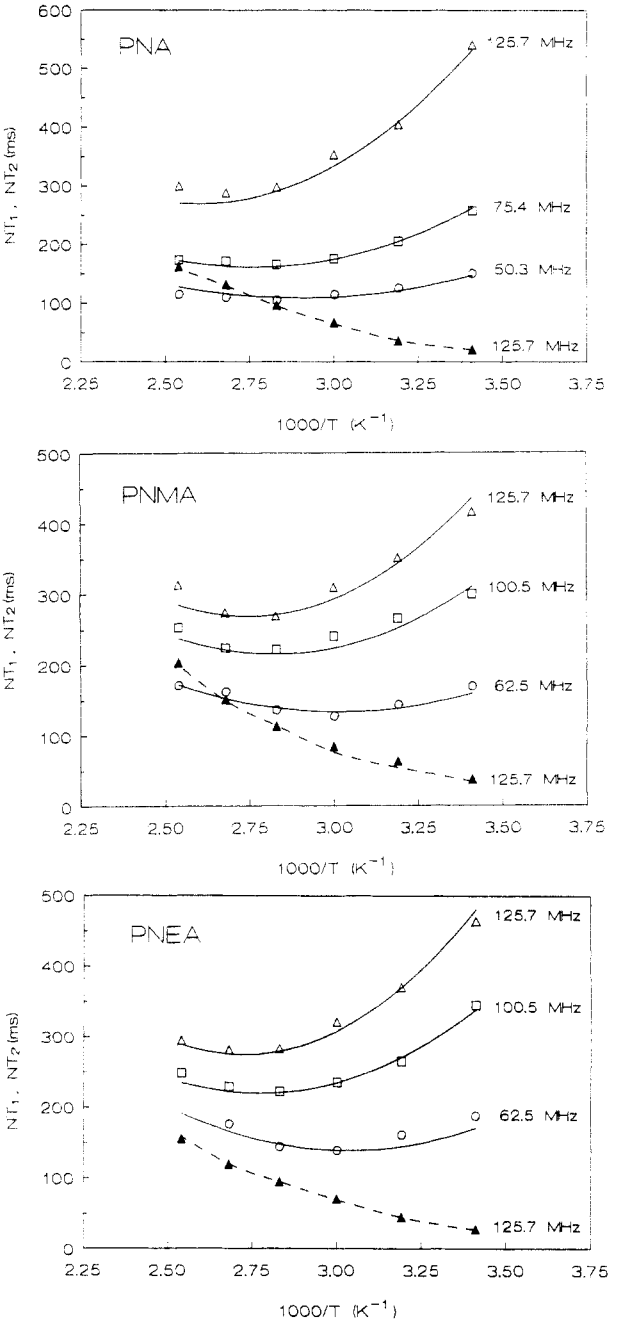

Figure 2. Experimental spin–lattice relaxation times (NT_1, open symbols), and spin–spin relaxation times (NT_2, filled symbols) for the backbone methine carbon of PNA, PNMA, and PNEA in TCE-d_2 solutions as function of temperature and magnetic field. Solid and dashed lines represent the best fit values calculated by using the DLM model.

of temperature in three magnetic fields. Also, these tables contain NT_2 values at high fields where relaxation contribution to the aromatic carbons from chemical shift anisotropy is more pronounced. As can be seen, the NT_1 values of the backbone methine carbons of the three polymers decrease with increasing temperature reaching a minimum as illustrated graphically in Figure 2. This demonstrates that these carbons experience motions which are within the "slow motion regime". As the temperature increases beyond the minimum, NT_1 values start increasing, indicating that motions characterized by short correlation times are contributing to the relaxation of the backbone carbons. The minima in the curves are shifted to higher temperatures (shorter correlation times) with increasing magnetic field in accord with relaxation theory[13,17] for isotropic motion. Moreover, NT_2 values at 125.7 MHz are smaller than NT_1 at all temperatures and decrease continually as temperature decreases (Figure 2). These features of the NT_1 and NT_2 values, and the fact that the NOE values are invariably below the extreme narrowing limit in the whole temperature range studied at the three fields (Tables 1–3), indicate that a single exponential TCF, i.e. isotropic motion, is inadequate to account for these relaxation data. Indeed, the relaxation times at the minima at all fields for the three polymer systems are twice as long as expected from the single-correlation time theory.

For both side-chain CH_2 carbons in PNEA, the NT_1 values increase monotonically with increasing temperature, and thus fall within the "fast motion regime" in all three

Table 1. ^{13}C Spin-Lattice Relaxation Times (NT_1, ms), Spin-Spin Relaxation Times (NT_2, ms), and NOE Values of Protonated Carbons of PNA in TCE-d_2 as a Function of Temperature and Magnetic Field

	magnetic field (MHz)											
	CH (bb)				*o*- and *m*-naphthyl				*p*-naphthyl			
	NT_1 (NOE)			NT_2	NT_1 (NOE)			NT_2	NT_1 (NOE)			NT_2
T (°C)	50.3	75.4	125.7	125.7	50.3	75.4	125.7	125.7	50.3	75.4	125.7	125.7
20	150	257	540	21	147	215	316	50	148	241	366	44
	(1.37)	(1.26)	(1.30)		(1.53)	(1.44)	(1.38)		(1.34)	(1.25)	(1.25)	
40	125	205	404	36	146	205	292	73	137	206	329	58
	(1.53)	(1.44)	(1.31)		(1.69)	(1.43)	(1.41)		(1.50)	(1.29)	(1.27)	
60	114	175	353	67	160	218	294	119	132	187	293	92
	(1.53)	(1.46)	(1.40)		(1.83)	(1.60)	(1.50)		(1.66)	(1.40)	(1.31)	
80	104	165	297	96	184	249	316	155	137	188	275	113
	(1.63)	(1.53)	(1.45)		(2.09)	(1.85)	(1.63)		(1.77)	(1.55)	(1.39)	
100	109	171	287	131	213	300	361	219	146	198	277	147
	(1.85)	(1.60)	(1.57)		(2.37)	(2.11)	(1.76)		(1.99)	(1.67)	(1.47)	
120	114	173	299	161	247	367	440	278	153	221	295	180
	(2.05)	(1.76)	(1.66)		(2.57)	(2.25)	(1.88)		(2.14)	(1.84)	(1.57)	

Table 2. ^{13}C Spin-Lattice Relaxation Times (NT_1, ms), Spin-Spin Relaxation Times (NT_2, ms), and NOE Values of Protonated Carbons of PNMA in TCE-d_2 as a Function of Temperature and Magnetic Field

	magnetic field (MHz)																
	CH (bb)					O–CH_2					*o*- and *m*-naphthyl				*p*-naphthyl			
	NT_1 (NOE)			NT_2		NT_1 (NOE)			NT_2		NT_1 (NOE)			$-T_2$	NT_1 (NOE)			$-T_2$
T (°C)	62.5	100.5	125.7	75.4	125.7	62.5	100.5	125.7	75.4	125.7	62.5	100.5	125.7	125.7	62.5	100.5	125.7	125.7
20	169	299	416	29	37	206	358	434	85	107	177	242	273	79	178	238	285	84
	(1.28)	(1.35)	(1.38)			(1.64)	(1.61)	(1.64)			(1.65)	(1.48)	(1.47)		(1.55)	(1.38)	(1.46)	
40	143	265	351	45	63	216	342	416	124	150	195	256	300		181	240	304	
	(1.45)	(1.45)	(1.30)			(1.68)	(1.65)	(1.65)			(1.83)	(1.69)	(1.52)		(1.73)	(1.65)	(1.44)	
60	127	240	309	61	84	234	382	444	172	212	241	303	345	164	210	275	317	162
	(1.56)	(1.49)	(1.45)			(1.93)	(1.95)	(1.94)			(2.09)	(2.17)	(1.72)		(1.89)	(2.00)	(1.64)	
80	136	221	269		113	280	438	488		290	317	388	422		254	333	363	
	(1.72)	(1.59)	(1.46)			(2.19)	(2.00)	(1.89)			(2.38)	(2.16)	(1.84)		(2.16)	(2.00)	(1.70)	
100	162	223	274		151	370	520	626		400	426	503	554	428	331	402	454	405
	(1.78)	(1.73)	(1.58)			(2.34)	(2.10)	(2.05)			(2.63)	(2.29)	(2.00)		(2.35)	(2.10)	(1.89)	
120	171	253	313		203	510	642	763		580		672	745			518	609	
	(1.80)	(2.02)	(1.90)			(2.57)	(2.47)	(2.24)			(2.72)	(2.45)	(2.14)		(2.49)	(2.16)	(2.07)	

magnetic fields. However, for the side-chain CH_2 carbon of PNMA, the NT_1 values pass through a minimum with increasing temperature. As expected this minimum shifts to higher temperatures with increasing magnetic field. At a given temperature and magnetic field, the relaxation times of the side-chain methylene carbons (moderated by two protons) are higher than the NT_1 values of the backbone methine carbons, and for PNEA, they tend to increase on going from the ester group toward the naphthyl moiety (Tables 2 and 3). This trend, which is more pronounced at higher temperature, is reminiscent of the relaxation behavior of hydrocarbon chains attached at one end to a heavy anchor,[33] i.e. an increasing internal mobility of the hydrocarbon chain toward its free end, owing to internal rotations about the C–C bonds. However, side-chain flexibility for PNEA is expected to be less pronounced than simple hydrocarbon chains due to the fact that the side chain in PNEA is anchored at both ends by the polymer backbone and the heavy naphthyl substituent.

The relaxation times of the C(2), C(3), C(6), and C(7) carbons of the naphthyl moiety on the one hand, and the relaxation times of the C(4), C(5), and C(8) on the other hand, are very similar for PNA at 20 and 40 °C, and for PNMA at 20 °C (Tables 1 and 2). At higher temperatures, however, the relaxation parameters of the former group of carbons become higher than those of the latter group. For PNEA, the relaxation times of the former group of carbons are higher than those of carbons of the latter group at all temperatures (Table 3). Moreover, the relaxation parameters in each group are similar within 5–10%, so that an average value of the relaxation parameters is considered in the present analysis and shown in Tables 1–3.

Several conclusions can be made from these observations. First, the rate of the naphthyl internal motion about the O–C(1) bond for PNA and the CH_2–C(1) bond for PNMA is slow at low temperature and becomes comparable or faster than the rate of the chain segmental motion at higher temperatures. Second, the rate of internal motion of the naphthyl group in PNEA is comparable or higher than the rate of the backbone segmental motion at all temperatures, a fact which is attributed to the additional flexibility introduced in the side chain by the second methylene group. Third, the fast internal motions about the O–C(1) and CH_2–C(1) bonds affect in a different way the relaxation of the two groups of the aromatic carbons of the naphthyl group, mentioned previously, as a consequence of the different orientations of their C–H internuclear vectors relative to the O–C(1) and CH_2–C(1) axes. A C–H vector parallel to O–C(1) and CH_2–C(1) axes will not be affected by internal rotation about these axes, whereas internuclear vectors making an angle of about 60° with these axes are expected to be influenced by internal rotation.[34]

It should be noted that additional flexibility within the ester group is expected to affect the rate of the side-chain motion. The effectiveness of these additional modes of reorientation is better reflected on the relaxation times of the C(4), C(5), and C(8) carbons of PNA at higher temperatures which are longer than those of the CH backbone carbon (Table 1). Normally, motions within the ester group are not amenable to an effective analysis

Table 3. ^{13}C Spin-Lattice Relaxation Times (NT_1, ms), Spin-Spin Relaxation Times (NT_2, ms), and NOE Values of Protonated Carbons of PNEA in TCE-d_2 as a Function of Temperature and Magnetic Field

	magnetic field (MHz)																					
	CH (bb)				O–CH_2				O–CH_2–CH_2				o- and m-naphthyl				p-naphthyl			
	NT_1 (NOE)			NT_2	NT_1 (NOE)			NT_2	NT_1 (NOE)			NT_2	NT_1 (NOE)			NT_2	NT_1 (NOE)			NT_2
T (°C)	62.5	100.5	125.7	125.7	62.5	100.5	125.7	125.7	62.5	100.5	125.7	125.7	62.5	100.5	125.7	125.7	62.5	100.5	125.7	125.7
20	188	345	464	28	216	352	438	106	244	350	444	150	181	234	277	152	168	234	271	164
	(1.32)		(1.36)		(1.72)		(1.75)		(1.69)		(1.71)		(1.78)	(1.54)	(1.58)		(1.55)	(1.51)	(1.46)	
40	161	265	370	45	234	368	456	174	278	400	484	240	217	283	317		177	248	293	
	(1.45)	(1.32)	(1.32)		(1.73)	(1.79)	(1.75)		(2.02)	(1.79)	(1.80)		(1.98)	(1.73)	(1.68)		(1.75)	(1.55)	(1.49)	
60	139	235	321	71	294	428	504	243	360	488	584	329	290	354	401	289	210	278	315	269
	(1.54)	(1.37)	(1.34)		(1.71)	(1.90)	(1.92)		(2.12)	(2.04)	(2.08)		(2.23)	(2.04)	(1.95)		(1.95)	(1.76)	(1.69)	
80	144	222	283	95	366	496	600	336	474	628	748	462	401	473	520		256	335	382	
	(1.67)	(1.47)	(1.46)		(1.87)	(1.92)	(2.00)		(2.31)	(2.25)	(2.26)		(2.47)	(2.18)	(2.08)		(2.17)	(1.93)	(1.84)	
100	176	229	281	119	420	566	694	430	624	818	908	594	521	630	665	477	324	413	456	367
	(1.76)	(1.65)	(1.48)		(2.09)	(2.02)	(2.19)		(2.50)	(2.45)	(2.36)		(2.64)	(2.40)	(2.26)		(2.45)	(2.14)	(2.01)	
120		248	294	155	556	726	852	600	854	1040	1148	850	747	853	892		436	528	566	
			(1.74)		(2.42)	(2.28)	(2.23)		(2.73)	(2.76)	(2.50)		(2.81)	(2.45)	(2.38)		(2.53)	(2.24)	(2.12)	

because of a lack of sufficient experimental data. Nevertheless, an effective rate of motion of this group can be simulated on the basis of the relaxation data of the para carbon of the PNA naphthyl group, whose relaxation is modulated only by this type of motion of the side chain.

Dynamic Modeling of Poly(1-naphthylalkyl acrylate)s

Modeling the dynamics of the three polymers, three general types of motion are considered: (1) the rotatory diffusion of the polymer chain as a whole, (2) backbone segmental motion, (3) side-chain motion. Each of these motions is considered as an independent source of motional modulation of the dipole–dipole interactions, so that the composite TCF can be written as a product of the TCF associated with each motion.

Overall Rotatory Diffusion. For sufficiently high molecular weight polymers, the overall motion is much slower than the chain local motions; hence, it is considered as a negligible contributor to the relaxation of the backbone carbons. The correlation time of the overall rotatory diffusion, τ_R, can be estimated at infinite dilution as a function of the molecular weight, M, and the intrinsic viscosity, $[\eta]$, of the polymer solution in a given solvent of viscosity, η_0, through the hydrodynamic equation[35]

$$\tau_R = \frac{2M[\eta]\eta_0}{3RT} \tag{14}$$

The estimated τ_R values were 3.2×10^{-6} s for PNMA, 4.9×10^{-6} s for PNEA at 30 °C. The same value for PNA was[7] 0.9×10^{-6} s at 30 °C. These values change only slightly,[11] considering a solution of finite concentration (10% w/v) and the effect of the molecular weight distribution of polymer samples. These long correlation times guarantee the preponderance of the chain local and internal motions as the major relaxation source for the protonated carbons of the polymers of the present study. The overall motion will not be considered in the rest of the calculations.

Backbone Segmental Motion. The first criterion for the validity of a chosen model is its ability to reproduce the relaxation data at the minimum of the NT_1 vs $1/T$ (K) curve. Table 4 summarizes the experimentally determined relaxation data for PNA, PNMA, and PNEA in TCE-d_2 for the three magnetic fields at a temperature where NT_1 exhibits a minimum value, and the calculated relaxation data derived by using the JS, HWH, and DLM models. As seen in Table 4, the JS and HWH models are unable to reproduce the multifield relaxation parameters of the three polymers at the NT_1 minimum. By contrast a very good fit is obtained by employing the DLM model, making it the best model, by far, in describing the backbone dynamics of the three polymers in solution. Hence, this model will be used for all subsequent calculations of the relaxation data.

The best fit NT_1 and NT_2 data over the whole temperature range studied for the backbone CH carbon of PNA, PNMA, and PNEA in TCE-d_2 by employing the DLM model is shown in Figure 2. It is clear from these plots that very good agreement between experimental and calculated values is obtained with this model throughout the entire temperature range studied. The ability of the DLM model to describe the chain segmental motion of the present polymer systems is supported by the NOE values. In some respects NOE experiments provide a more stringent test of motional models than do relaxation times.[36] Figure 4 show the experimental NOEs for the backbone CH carbon of the three polymers at the three

Table 4. Experimental and Calculated (JS, HWH, and DLM Models) ^{13}C NT_1 (ms), NT_2 (ms), and NOE Values of the Backbone Methine Carbon of PNA, PNMA, and PNEA in TCE-d_2 for Three Magnetic Fields at the Temperature at Which NT_1 Exhibits a Minimum Value

	PNA						
	50.3 MHz		75.4 MHz		125.7 MHz		
	NT_1	NOE	NT_1	NOE	NT_1	NT_2	NOE
expt	104	1.63	165	1.53	297	96	1.45
JS	93	1.68	142	1.59	262	90	1.45
HWH	98	1.82	142	1.64	241	88	1.42
DLM	109	1.63	163	1.50	288	95	1.43
	PNMA						
	62.5 MHz		100.5 MHz		125.7 MHz		
	NT_1	NOE	NT_1	NOE	NT_1	NT_2	NOE
expt	136	1.72	221	1.59	269	113	1.46
JS	137	1.87	218	1.79	274	100	1.71
HWH	126	1.87	192	1.66	240	106	1.56
DLM	137	1.74	216	1.54	272	114	1.46
	PNEA						
	62.5 MHz		100.5 MHz		125.7 MHz		
	NT_1	NOE	NT_1	NOE	NT_1	NT_2	NOE
expt	144	1.67	222	1.47	283	95	1.46
JS	136	1.84	219	1.71	276	84	1.62
HWH	128	1.85	197	1.64	246	90	1.54
DLM	141	1.70	225	1.50	285	95	1.42

Table 5. Simulation Parameters of the DLM Model Used To Describe Backbone Segmental Motions of PNA, PNMA, and PNEA in TCE-d_2

	τ_1 (ns)		
T (°C)	PNA	PNMA	PNEA
20	12.14	5.14	5.40
40	6.63	3.06	3.18
60	3.49	2.02	1.88
80	2.18	1.18	1.27
100	1.41	0.77	0.92
120	1.03	0.46	0.60
τ_0/τ_1	3	5	7
τ_1/τ_2	30	50	70
θ_{CH}°	22.9	18.9	19.2
E_a (kJ mol^{-1})	24	23	21
τ_∞ (10^{-12} s)	0.6	0.5	1.1
r	0.999	0.996	0.999

magnetic fields covering a temperature range of 100 °C. The curves show the prediction of the DLM model. The agreement between the 54 experimental values, and the calculated NOE values is almost quantitative.

The values of the fitting parameters of the DLM model for the three polymers are summarized in Table 5. A salient feature of these figures is that the correlation times, τ_1, for backbone cooperative transitions are very similar for PNMA and PNEA and shorter by a factor of 2 than the corresponding correlation time of PNA. This indicates a faster backbone rearrangement for the former polymers, and hence an increasing chain flexibility relative to the PNA main chain. However, the activation energy for the backbone motion in the three polymers, obtained from the Arrhenius plot of the corresponding τ_1 values, are not very different within experimental error. The ratio τ_0/τ_1 appears to increase from PNA to PNEA (Table 5), indicating that single conformational transitions associated with damping play a lesser role on going from PNA to PNEA polymer.

Another interesting observation is the fact that the τ_1/τ_2 ratio increases progressively from PNA to PNEA (Table 5) reflecting an increasing rate of the librational motion of the backbone C–H vector from PNA to PNEA. This result is in agreement with the observed best fit half-angle, θ, of the librational motion, which decreases from 23° for PNA to 19° for PNMA and PNEA (Table 5). A smaller half-angle corresponds to a shorter correlation time for the librational motion.[12]

The value of θ, for the C–H vector at the backbone methylene carbon site of PNA is greater than that calculated for the C–H vector of the backbone methine group of the same polymer (29° vs 23°). Although the relaxation data for the methylene carbon are not determined with the same accuracy as those of the methine carbon, and calculations were performed by using data at one field only, this result supports the conclusion observed

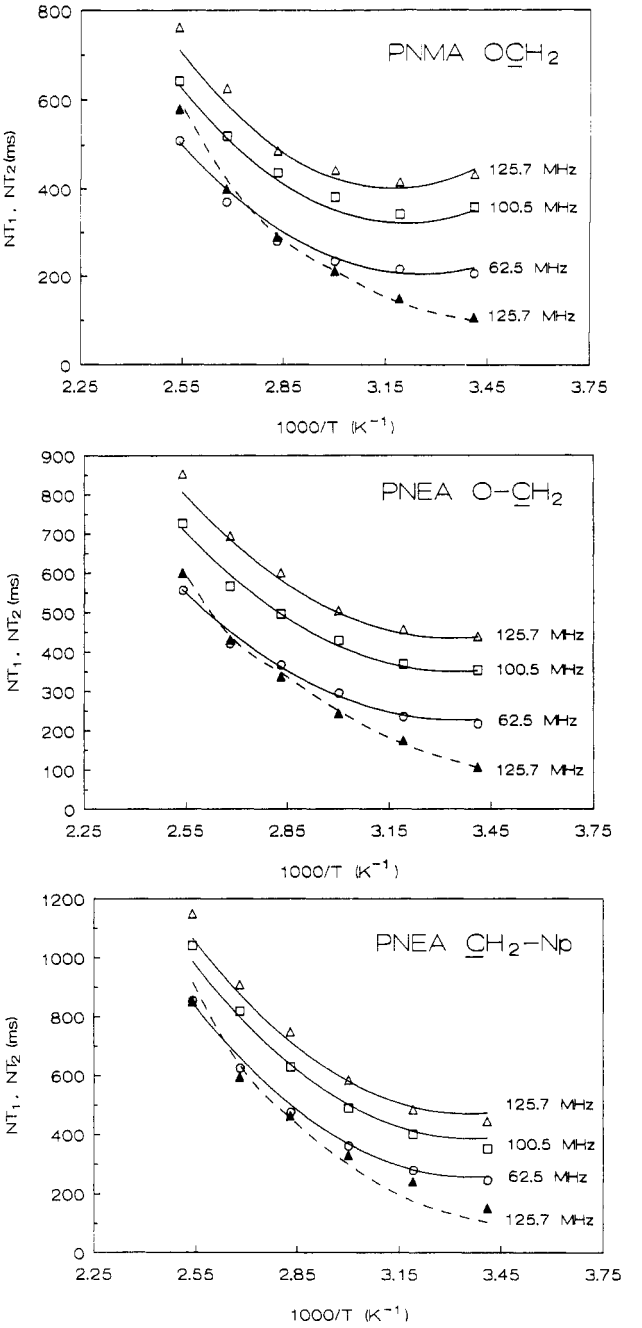

Figure 3. Experimental spin–lattice relaxation times (NT_1, open symbols), and spin–spin relaxation times (NT_2, solid symbols) for the side-chain methylene carbons of PNMA and PNEA in TCE-d_2 solutions as a function of temperature and magnetic field. Solid and dashed lines represent the best fit values calculated by using the restricted multiple internal rotations model.

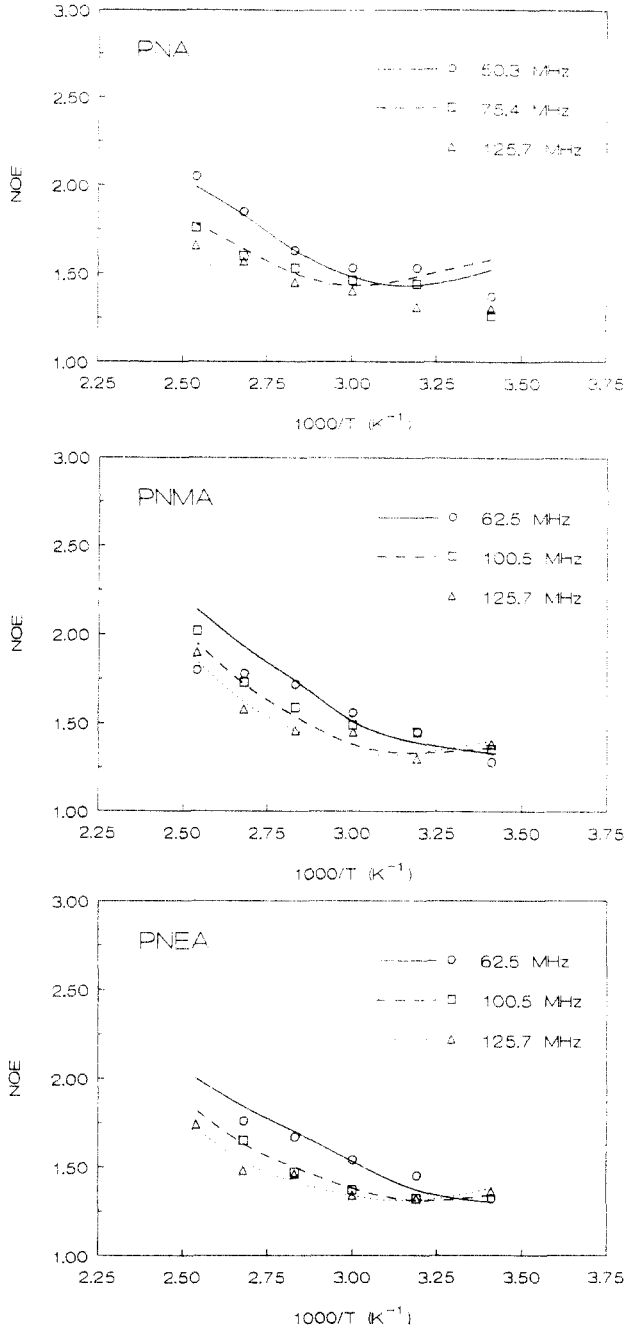

Figure 4. Experimental NOE values for the backbone methine carbon of PNA, PNMA, and PNEA in TCE-d_2 solutions as function of temperature and magnetic field. Solid, dashed, and dotted lines represent the best fit values calculated by using the DLM model.

in other polymers,[12,23,25,36-38] namely that a smaller θ value for the CH group indicates a greater steric hindrance to the librational motion of the C–H vector relative to that in the CH_2 group. The methine carbon has a directly attached side chain which, because of its size, physically restricts the amplitude of the local libration.

It is of interest to compare the activation energy, E^*, of the conformational transitions in the polymer chain, which can be estimated from the apparent activation energy, E_a, obtained from relaxation data (Table 5), by subtracting the activation energy, ΔH_η, for solvent viscosity, i.e.

$$E^* = E_a - \Delta H_\eta \tag{15}$$

This equation is based on Kramers' theory[39] for the diffusion of a particle over a potential barrier. According to this theory, the correlation time associated with a motional mode involving the crossing of an energy barrier E^* in a hydrodynamic regime governed by viscous friction can be written as

$$\tau = B\eta_0 e^{-E^*/RT} \tag{16}$$

where η_0 is the solvent viscosity and B is a molecular constant. ΔH_η for TCE was found to be[40,41] 12 kJ mol^{-1}. This value leads to a value for E^* of 12 kJ mol^{-1} for PNA, 11 kJ mol^{-1} for PNMA, and 9 kJ mol^{-1} for PNEA.

Kramers' theory was the basis of a theoretical treatment of conformational transitions occurring in a polymer chain made by Helfand.[42] He classified polymer cooperative motions into two general types: Type 1 motion, a crankshaft conformational transition about two collinear bonds in which the positions of the chain ends remain unchanged during rotation, and type 2 motion, a cooperative transition resulting in a translational motion of the chain ends. Although the displacement of the chain ends involved in a type 2 motion makes it less favorable than a type 1 motion, a smaller activation energy is associated with the former. In fact the activation energy for a type 2 motion is only slightly greater than the barrier (8–10 kJ mol^{-1}) separating the trans and gauche states. Since a type 1 motion involves simultaneous rotations about two coaxial backbone bonds, it involves on the average two barrier crossings (ca. 20 kJ mol^{-1}), i.e. twice the energy barrier for the trans-gauche transition. The present experiments indicate activation energies for segmental motion of the three polymers equal or slightly greater than one barrier crossing, indicating that in TCE-d_2, type 2 motions predominate.

Ediger and co-workers[40,43] have shown recently that the use of Kramers' theory in the high friction limit is an assumption which can be very seriously in error, especially for solvents of high viscosity. For polymer systems where polar polymer/solvent interactions are absent, Kramers' theory can break down. In this case, the viscosity dependence of motional rates (eq 16) is not linear and the potential barrier of the local chain motions is essentially independent of solvent viscosity. Therefore, the difference between activation energies as expressed by eq 15 may not be applicable for the present polymer systems. To resolve this ambiguity we extended our ^{13}C relaxation measurements on PNMA in additional nonpolar solvents.[44] These additional experimental data and subsequent analysis showed[44] that Kramers' theory is valid for the present polymer systems.

Frequency–Temperature Superposition. Recently, Guillermo et al.[45] have demonstrated a method for superimposing NT_1 data collected at different Larmor frequencies. The success of such a superposition indicates that the shape of the TCF used to interpret the relaxation data is temperature independent, and that the mechanisms of chain local motions reflected in the TCF are independent of temperature. This superposition is possible only if the time constants that enter into the explicit expression of the TCF have the temperature dependence of a characteristic constant, $\tau(T)$. A plot of $\log(\omega_C/NT_1)$ vs $\log[\omega_C\tau(T)]$, as suggested by Ediger,[46] successfully superposes the ^{13}C relaxation data from different Larmor frequencies. This indicates both that the TCF has a shape independent of temperature, and that the calculated temperature dependence is correct.

We have applied a similar procedure to our NT_1 data, and plot $\log(\omega_C/NT_1)$ vs $\log[\omega_C\tau_1(T)]$. Figure 5 shows these plots for the methine backbone carbon of the three polymers. Data from three Larmor frequencies superpose very well over the entire temperature range. This

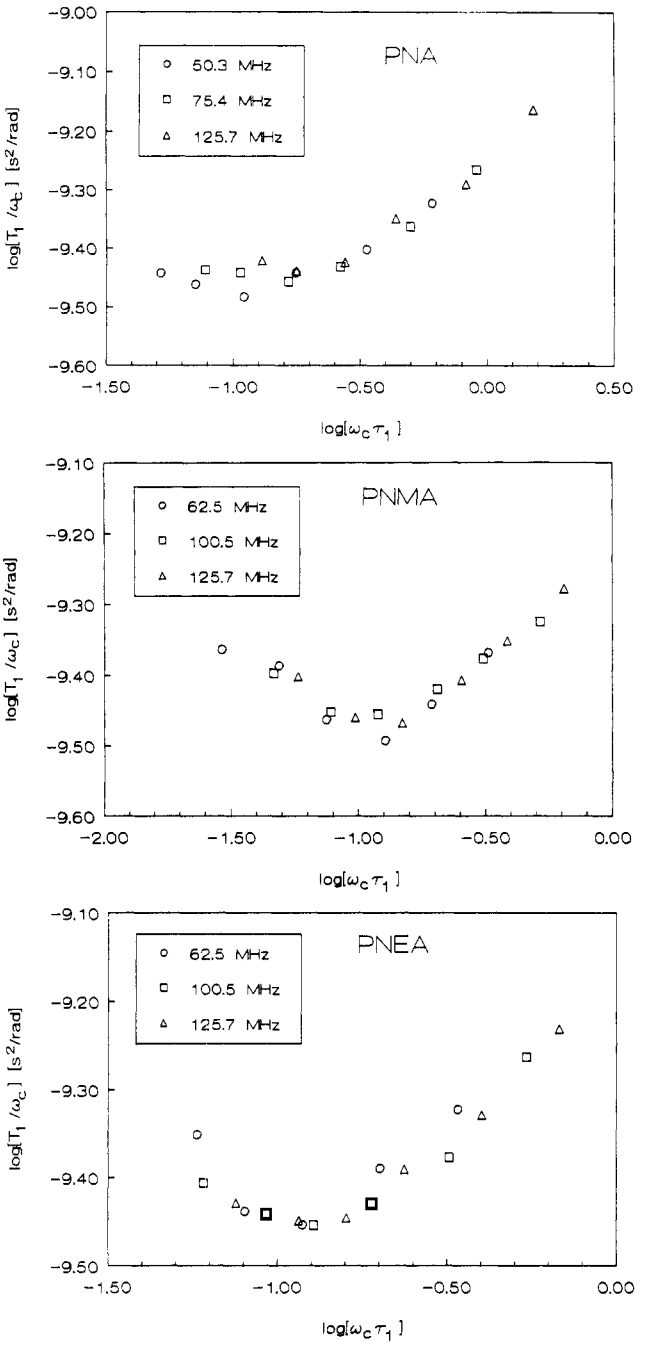

Figure 5. Frequency–temperature superposition of ^{13}C NMR NT_1 values for the backbone methine carbons of PNA, PNMA, and PNEA in TCE-d_2 solutions. τ_1 values are the correlation times obtained from the analysis of the relaxation data by using the DLM model (Table 5). The symbols correspond to different Larmor frequencies, $\omega_C/2\pi$.

demonstrates that all of the motional time constants contributing to spin relaxation are proportional to $\tau_1(T)$, and justifies attempts to fit the data to the DLM model.

Side-Chain Motion. The relaxation data of the side chains of the three polymers given in Tables 1–3 were analyzed by using the spectral density function of eqs 12 and 13 describing restricted rotations superimposed on backbone segmental motion. To facilitate this analysis, we have made the following clarifications and simplifying assumptions:

(1) The only relaxation mechanism considered for the side-chain methylene carbons is the ^{13}C–^{1}H dipole–dipole interactions. However, the contribution of the CSA mechanism to the relaxation of the aromatic carbons cannot be ignored especially at high fields, and therefore, eqs 6–9 should be used for the analysis of their relaxation parameters.

(2) All internal motions of the side chains are considered to be independent. This assumption may be unrealistic for longer side chains, where hydrodynamic effects may cause concerted type motions to occur, involving partial rotations about several bonds. For shorter chains and for free internal motions, this deficiency is not severe. For restricted internal rotations this assumption is valid only for relatively large angular amplitudes.

(3) Internal rotations within the ester groups are effective in modulating local magnetic fields, and thus are expected to cause relaxation of the side-chain methylene and naphthyl carbons. Theoretical studies[47,48] for poly(alkyl methacrylate)s suggest that the barrier to rotation about the C–CO bond is ~30 kJ mol^{-1}, and it is much reduced for poly(methyl acrylate) to ~20–22 kJ mol^{-1}.[48] By contrast, the barrier about the O–CO bond is expected to be very large, owing to conjugation effects such as those leading to high barriers in amides. Indeed, theoretical calculations gave[47,48] 62 kJ mol^{-1} for poly(methyl methacrylate), 113 kJ mol^{-1} for poly(*tert*-butyl methacrylate), and 50 kJ mol^{-1} for poly(methyl acrylate). Experimental and theoretical studies[49] in aliphatic esters and carboxylic acids suggest a barrier of ca. 45 kJ mol^{-1} for rotation about the O–CO bond. The other type of bond in the ester group, which should be particularly susceptible to internal rotation is the O–CH_2 bond in PNMA and PNEA, or the O–C(1) bond in PNA. The barrier to rotation about that bond is ca. 5 kJ mol^{-1} for poly(alkyl methacrylate)s and poly(methyl acrylate).[47,48]

(4) Individual bond rotations inside the ester group cannot be treated quantitatively due to the lack of sufficient relaxation data as mentioned earlier. However, the cumulative effect of rotations about the ester bonds on the relaxation of the side chain carbons can be estimated from the relaxation data of the C(4), C(5), and C(8) carbons of PNA. As pointed out earlier, these carbons are not relaxed by rotation about the O–C(1) bond, but they do receive relaxation contribution from bond rotations within the ester group.

The best fit NT_1, NT_2, and NOE values for the side-chain methylene carbons of PNMA and PNEA are shown in Figures 3 and 6 by the solid and dashed lines. Very good agreement between experimental and calculated values is obtained from the model of restricted internal rotations throughout the entire temperature range studied. Table 6 summarizes the fitting parameters for this model. The theoretical data in Figures 3 and 6 were obtained by introducing an additional restricted motion, which represents the cumulative bond rotations inside the ester group. The calculated apparent diffusion constant for the ester group, D_{ester}, from the average relaxation data of the C(4), C(5), and C(8) carbons of the naphthyl group in PNA (Table 1) were found to be slightly dependent on temperature, whereas the angle, $2\varphi_{ester}$, varied between 60° and 100°. The D_{ester} values showed a linear dependence on $1/T$ (correlation coefficient = 0.92) in the corresponding Arrhenius plot, giving an activation energy of ~20 kJ mol^{-1}. These values compare favorably with the energy barrier (20–30 kJ mol^{-1}), and the range of oscillation (~120°) calculated for the rotation of the $-COOCH_3$ group in poly(methyl acrylate) and poly(methyl methacrylate).[47,48]

The diffusion constants, D_1, for rotation about the O–CH_2 bond in PNMA and PNEA are very similar and they increase with increasing temperature (Table 6). The diffusion constant, D_2, for rotation about the CH_2–CH_2 bond in PNEA is 3–4 times smaller than D_1 for the same

Table 6. Simulation Parameters[a] of the Restricted Multiple Internal Rotations Model Used To Describe Side Chain (Methylene and Naphthyl Groups) Motions of PNA, PNMA, and PNEA in TCE-d_2

	PNA		PNMA				PNEA					
T (°C)	D_{np}	φ_{np}°	D_1	φ_1°	D_{np}	φ_{np}°	D_1	φ_1°	D_2	φ_2°	D_{np}	φ_{np}°
20			5.66	53	0.188	43	5.66	57	1.83	40		
40	0.200	33	7.28	55	0.483	38	7.72	63	2.46	47	0.137	133
60	0.445	36	9.78	52	1.273	56	11.38	69	3.27	56	0.147	129
80	0.998	43	12.20	62	2.334	62	16.69	77	4.43	62	0.207	129
100	1.625	50	16.22	75	3.246	69	18.27	88	6.22	66	0.330	130
120	2.778	51	21.60	75	5.522	70	22.33	128	6.63	69	0.384	137
E_a (kJ mol^{-1})	34		13		32		14		13		15	
D_∞ (10^{12} s)	88		0.98		114		1.67		0.38		0.033	
r	0.998		0.995		0.994		0.992		0.994		0.968	

[a] D_i's × 10^9 s^{-1}.

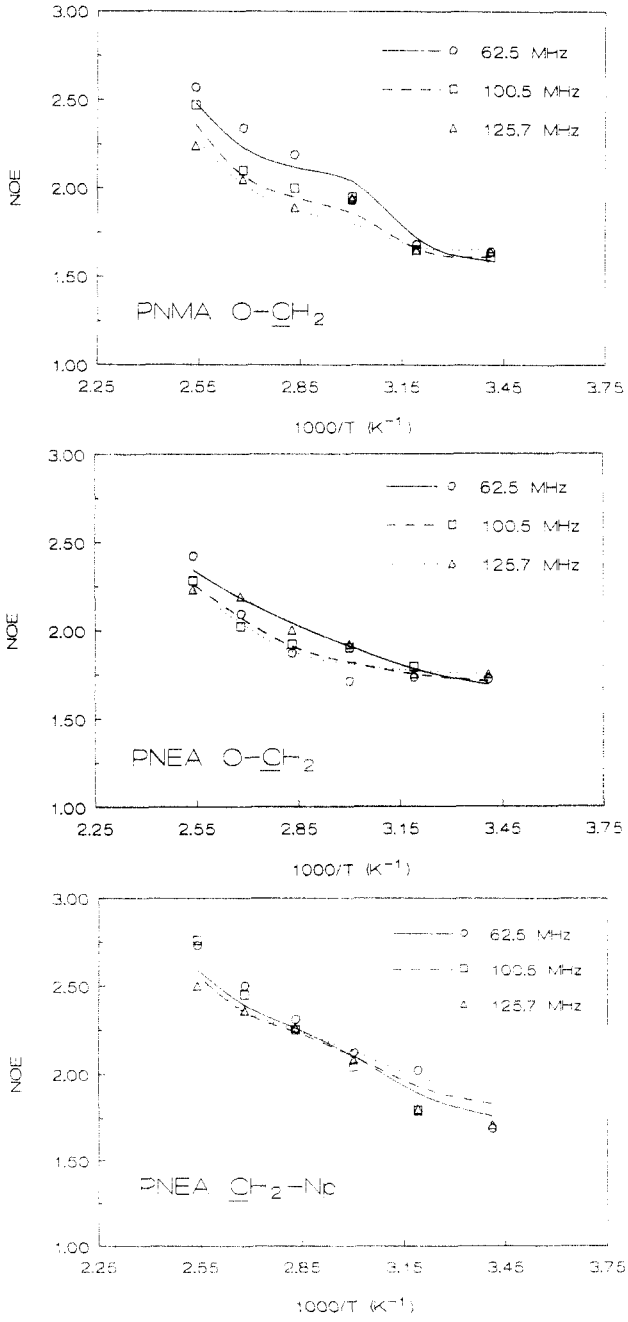

Figure 6. Experimental NOE values for the side-chain methylene carbons of PNA, PNMA, and PNEA in TCE-d_2 solutions as function of temperature and magnetic field. Solid, dashed, and dotted lines represent the best fit values calculated by using the restricted multiple internal rotations model.

polymer indicating a slower motion about the CH_2–CH_2 bond than about the O–CH_2 bond. However, the calculated activation energies for rotations about these bonds are the same (Table 6). A plausible explanation of this observation is based on the fact that the bulky naphthyl moiety, which anchors the other end of the side chain, hinders the internal motion of the adjacent methylene group. This effect is also reflected on the smaller angular amplitude, $2\varphi_2$, for restricted rotation about the CH_2–CH_2 bond in PNEA relative to $2\varphi_1$ for restricted rotation about the O–CH_2 bond.

The simulation parameters for the naphthyl internal rotation of the three polymers are displayed in Table 6. Figure 7 illustrates the best fit of the average NT_1 and NT_2 values for the C(2), C(3), C(6), and C(7) carbons. Agreement between experimental and calculated values is very good. Also, good agreement within ±10% was obtained for the NOE values. The rates of naphthyl internal motion for all polymer systems, reflected on the diffusion constants, D_{np} (Table 6), are faster by 1 order of magnitude than the backbone motion (τ_1 values in Table 5). Comparison of the D_{np} values and angular amplitudes in Table 6 reveals a slower, but less restricted naphthyl internal motion from PNA and PNMA to PNEA polymer. The amplitude $2\varphi_{np}$ increases slightly with temperature from 60° to 100° for PNA, and from 80° to 140° for PNMA. For PNEA, it is constant and equal to ~260°. The calculated activation energies from the Arrhenius plots of the D_{np} values are similar in PNA and PNMA, and greater by a factor of 2 than that in PNEA (Table 6).

Discussion

Carbon-13 relaxation data of the backbone methine carbons of PNA, PNMA, and PNEA in TCE-d_2 solutions have been modeled by using three different models. Among these the JS and HWH models failed to account for the relaxation parameters at the NT_1 minimum in the curve of NT_1 versus temperature. Also, these models failed at all temperatures to reproduce the experimental relaxation data. This is contrary to what was observed in an earlier publication,[7] where both models appeared to fit the experimental data of PNA in TCE-d_2 solution at two magnetic fields. Nevertheless, this fitting was achieved by using a rather high value of 1.11 A for the backbone C–H distance. The conventional value of 1.09 A offered a bad quality of the fitting and unreasonable simulation parameters for both models, as observed in the present study as well. Moreover, additional relaxation experiments, including T_2 measurements, have been performed in the present study offering a larger set of data to test more efficiently the various dynamic models.

Results obtained in this study indicate that the introduction of a librational motion for the backbone C–H vector into the correlation function of the HWH model is an important factor in order to interpret the backbone

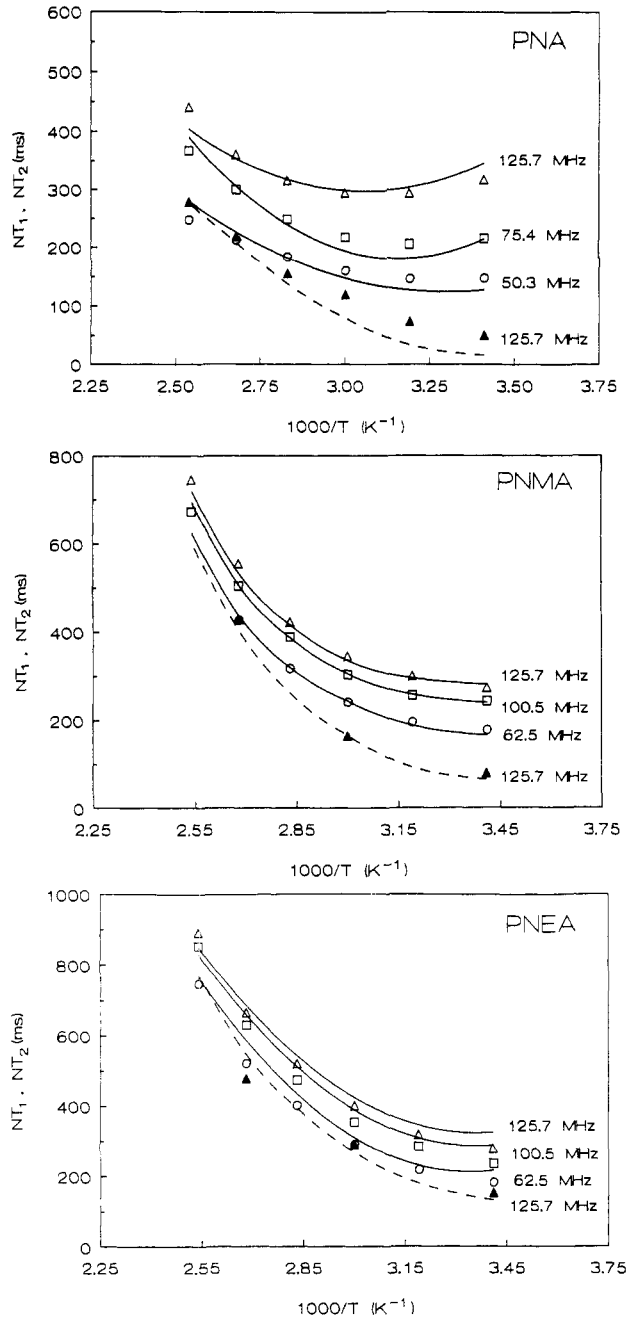

Figure 7. Experimental average spin–lattice relaxation times (NT_1, open symbols), and spin–spin relaxation times (NT_2, solid symbols) for the C(2), C(3), C(6), and C(7) carbons of the naphthyl group of PNA, PNMA, and PNEA in TCE-d_2 solutions as a function of temperature and magnetic field. Solid and dashed lines represent the best fit values calculated by using the restricted multiple internal rotations model.

relaxation data of the present polymer systems. This motion is very rapid and accounts for ca. 15–25% of the correlation function decay of the CH carbon as estimated from the parameter A in eqs 10 and 11. Backbone conformational transitions are responsible for the remaining decay of the correlation function.

The reason underlying the failure of the HWH model to describe segmental dynamics of the present polymer systems may be found[46] in the lack of a clean separation in the time scale between τ_0 and τ_1 correlation times, as reflected on the calculated τ_0/τ_1 ratios, which assume values between 3 and 7 (Table 5). On the other hand, the DLM model, describing backbone conformational and librational motions in two distinct time scales consistently provides excellent agreement with the experiment.

Conformational and librational motions are separated in time scale by a factor of 30–70 for the present polymers (Table 5). This separation is much smaller, and thus less distinct, than that observed in previous work[12,23,25,36–38,46] where the conformational and librational motions are separated in time scale by a factor of 200 or greater. This implies that the ratios τ_1/τ_2 may be determined to a better accuracy for the present polymers. Nevertheless, the librational motions are still very rapid to be considered as thermally activated processes. If τ_2 is essentially independent of temperature, it can be as large as 4×10^{-10}, 1×10^{-10}, 8×10^{-11} s at 20 °C for PNA, PNMA, and PNEA, respectively.

The amplitudes, 2θ, of the librational motions determined from relaxation data at the minima are within the range 30–60° observed for most polymers in solution and in the bulk. The cone of angles available for libration of a given C–H vector presumably reflects contributions from at least the two neighboring torsional angles, thus justifying the major hypothesis of the DLM model[23] that this anisotropic motion occurs within a torsional potential well.[46]

The superposition of NT_1 data in Figure 5 demonstrates that the shape of the correlation function describing conformational transitions does not change with temperature. The fact that a single correlation time is sufficient to describe conformational transitions indicates that the length scale of cooperativity within the polymer chain must be small. Indeed, the values of τ_0/τ_1 ratios in Table 5 for the present polymer systems reflect a narrow width of distribution of time constants describing conformational dynamics. In this respect, it is interesting to note that Brownian dynamics simulation of local motions in polyisoprene has shown[41] that conformational transitions are localized to about one repeat unit.

The sidechain motions including naphthyl internal rotation have been described in terms of two phenomenological parameters, the rate of the internal diffusion about the "exo-backbone" bonds, D_i, and the amplitude of the restricted internal motions, $2\varphi_i$. The results of this study indicate that if one neglects the angular restriction and makes $2\varphi_i = 360°$, i.e. essentially the free diffusion model, an effective D_i cannot be chosen to account for the frequency dependence of the relaxation data. Similar conclusions have been reached by other investigators[27,50–52] studying side-chain motions in polymer systems.

Comparison of the motional parameters for the three polymers summarized in Tables 5 and 6 reveals a number of differences and similarities regarding the dynamics of these systems. The time scale for cooperative transitions expressed by τ_1 is slower by a factor of 2 in PNA than in PNMA and PNEA, the latter polymers being characterized by similar τ_1 values. The activation energies associated with τ_1 are nearly the same for the three polymers (Table 5). This reflects the similar influence of the solvent viscosity on their segmental motion. As a result, and following Kramers' theory, the same type of conformational transitions, namely type 2 according to Helfand's notation, prevails in all types of polymer chains of the present systems. However, there is a slight difference among the rates and the extent of the librational motions of the backbone C–H vectors in the three polymers. The cone half-angle θ of 23° for PNA is greater than the value of 19° observed for both PNMA and PNEA (Table 5). This observation indicates a greater steric hindrance to the librational motion of the C–H vectors in the latter polymers, which may be attributed to the increasing size of the side chain in PNMA and PNEA.

The activation energies of internal rotations of the side chain methylene groups for PNMA and PNEA are nearly identical (Table 6), although the prefactors, D, and the angular amplitudes of restricted rotations depend on the position of each methylene group in the side chain. In particular, the saturated side chain of PNEA is anchored at both ends, and the observed differences in rates and amplitudes between the two methylene groups (Table 6) reflect differences in nonbonded interactions from the adjacent ester and naphthyl moieties.

The naphthyl group rotation has been best modeled by a restricted internal diffusion process about the terminal bond of the side chain. Naphthyl internal rotation in PNA is a factor of about 2 slower at a given temperature relative to PNMA as reflected on the D_{np} values in Table 6. Also, the angular amplitude ($2\varphi_{np}$) of restricted rotation in PNA is smaller than that in PNMA. However, the activation energies for this internal motion are very similar in the two polymers. On the other hand, the naphthyl rotation in PNEA is much slower, but less restricted, than in the other two polymers at each temperature. This behavior is reflected on the smaller diffusion constants and larger amplitudes of PNEA than those of PNA and PNMA in Table 6. These observations may indicate that the mechanism of naphthyl rotation is the same for PNA and PNMA, but not for PNEA.

Another interesting observation is the fact that the activation energy for naphthyl rotation in PNEA is about one-half of the activation energy of PNA and PNMA. Factoring out the solvent effect, which should be the same for the three polymers, the higher activation energy observed in the latter polymers may be attributed to the presence of severe constraints to the naphthyl internal motion imposed by neighboring bulky chromophores. It appears that the presence of an additional methylene unit in the side chain of PNEA increases its flexibility enough to accomodate more easily the internal rotation of the naphthyl moiety in PNEA.

Correlation of Polymer Microstructure and Polymer Dynamics with Photophysical Results. In a previous publication,[3] the photophysical behavior of an analogous series of poly(1-naphthylalkyl methacrylate)s was correlated to their microstructure. However, the lack of a backbone CH carbon and the very broad CH_2 resonance of the main polymer chains prevented the establishment of correlation, if any, between photophysical results and dynamic properties of these polymer systems. This correlation is possible for the present polymers for which both microstructure and dynamic properties are known. The microstructure of these polymers has been determined[6] from their corresponding ^{13}C NMR spectra. The splitting of the various carbon resonances has shown[6] that they are heterotactic polymers conforming with Bernoullian statistics. On the basis of the calculated probability of generating meso sequence (P_m) at the end of the growing chain, the isotacticity appears to be similar for the present polymers, namely P_m(PNA) = 0.40, P_m(PNMA) = 0.43, and P_m(PNEA) = 0.39.

Although photophysical results exist only for the first member of the series, i.e. PNA[53,54] the photophysical behavior along the series is expected to parallel that of the analogous poly(1-naphthylalkyl methacrylate)s.[53-57] The main difference comparing poly(1-naphthylalkyl acrylate)s with poly(1-naphthylalkyl methacrylate)s is that the backbones of the former polymers are more flexibile than those in the latter series, leading to a more efficient trapping of electronic energy at the excimer-forming step.[53]

Assuming that the excimer formation in poly(1-naphthylalkyl acrylate)s follows the same order as in poly(1-naphthylalkyl methacrylate)s,[53-57] i.e. PNA > PNMA ≈ PNEA, it appears that the decrease in monomer emission (increasing tendency to excimer formation) with decreasing side-chain length, on going from PNEA to PNA, is not affected by tacticity, since these polymers are characterized by nearly the same isotacticity as mentioned previously.

Apart from polymer microstructure, which reflects the local density of the naphthalene chromophores along the polymer backbone, the excimer-forming step involves backbone and side-chain rotations to adopt the pertinent conformation in which the chromophores overlap extensively in a plane–parallel fashion. Moreover, the conformational changes of the backbone chain and side-chain motions must be always faster than the excimer-forming step.[58] The analysis of the ^{13}C NMR relaxation data of the present polymers show that the rates of the backbone segmental motion in TCE-d_2 of these polymers are smaller than the rate of excimer formation. For PNA, the rate of excimer formation, k_{DM}, is 1.2×10^9 s^{-1} in EtOAc, and 1×10^9 s^{-1} in CH_2Cl_2 at 23 °C,[53] whereas the rate of backbone motion of the same polymer in TCE-d_2, expressed in terms of the diffusion constants ($D = 1/6\tau_1$), is 1.4×10^7 s^{-1} at 20 °C (Table 5). Although TCE solvent is more viscous than EtOAc and CH_2Cl_2 solvents [η(TCE) = 1.785, η(EtOAc) = 0.455, and $\eta(CH_2Cl_2)$ = 0.433 cP at 20 °C], in which photophysical experiments were carried out, this difference in solvent viscosity is not expected to increase the rate of the backbone motion by 2 orders of magnitude. Indeed, the rate of the backbone motion for PNMA calculated from ^{13}C relaxation experiments[44] in $CDCl_3$, whose viscosity [$\eta(CDCl_3)$ = 0.563 cP at 20 °C] is close to those of EtOAc and CH_2Cl_2, was found to be 1.1×10^8 s^{-1}, while a value of 3.2×10^7 s^{-1} was found in TCE-d_2 at 20 °C for the same polymer (Table 5). From this discussion, it appears that backbone segmental motion plays a minor role in the excimer formation in these polymer systems.

The rates of the side-chain motion and, in particular, those of the naphthyl internal rotations are at least comparable to the rates of excimer formation. For PNMA, $D_{np} = 1.9 \times 10^8$ s^{-1} in TCE-d_2 (Table 6) and 1.5×10^9 s^{-1} in $CDCl_3$ at 20 °C.[44] This indicates that side-chain motion is an important factor for excimer formation. Moreover, the higher activation energies and the smaller amplitudes of the restricted internal motion in PNA and PNMA (Table 6) appears to confine excimer formation between nearest naphthyl groups, while the lower activation energy and the much less restricted motion in PNEA allows excimer formation, between next neighbor naphthyl moieties in addition to nearest naphthyl groups.

Acknowledgment. We gratefully acknowledge financial support from the British Council and NATO (grant no. CRG 910406). SERC (U.K.) provided funding for the 500-MHz instrument.

References and Notes

(1) Guillet, J. E. *Polymer Photophysics and Photochemistry*, Cambridge University Press: Cambridge, U.K., 1985.
(2) Semerak, S. N.; Frank, C. W. *Adv. Polym. Sci.* **1983**, *54*, 33.
(3) Radiotis, T.; Spyros, A.; Dais, P. *Polymer* **1993**, *34*, 1846.
(4) Renamayor, C. S.; Gomez-Anton, M. R.; Calafate, B.; Mano, E. B.; Radic, D.; Gargallo, L.; Freire, J. J.; Pierola, I. F. *Macromolecules* **1991**, *24*, 3328.
(5) Chakraborty, D. K.; Heitzhauss, K. D.; Hamilton, F. J.; Harwood, H. J.; Mattice, W. L. *Macromolecules* **1991**, *24*, 75.
(6) Spyros, A.; Dais, P.; Heatley, F. *Makromol. Chem.*, in press.
(7) Spyros, A.; Dais, P. *Macromolecules* **1992**, *25*, 1062.
(8) Meiboom, S.; Gill, D. *Rev. Sci. Instrum.* **1958**, *29*, 688.

(9) Ernst, R. R. *J. Chem. Phys.* **1966**, *45*, 3845.
(10) Craik, D. J.; Kumar, A.; Levy, G. C. *J. Chem. Int. Comput. Sci.* **1983**, *1*, 30.
(11) Dais, P. *Carbohydr. Res.* **1987**, *160*, 73.
(12) Radiotis, T.; Brown, G. R.; Dais, P. *Macromolecules* **1993**, *26*, 1445.
(13) Farrar, T. C. *An Introduction to Pulse NMR Spectroscopy*; Farragut Press: Chicago, 1987.
(14) The preponderence of dipole–dipole relaxation mechanism relative to other mechanisms for protonated and nonprotonated saturated carbons has been examined: Gutnell, J. D.; Glasel, J. A. *J. Am. Chem. Soc.* **1977**, *99*, 42.
(15) Doddrell, D.; Glushko, V.; Allerhand, A. *J. Chem. Phys.* **1972**, *56*, 3683.
(16) Pople, J. A.; Gordan, M. J. *J. Am. Chem. Soc.* **1967**, *89*, 4253.
(17) Abragam, A. *The principles of Nuclear Magnetism*; Clarendon Press: Oxford, 1961; Chapter VIII.
(18) Sherwood, M. H.; Facelli, J. C.; Alderman, D. W.; Grant, D. M. *J. Am. Chem. Soc.* **1991**, *113*, 750.
(19) Heatley, F. *Progr. NMR Spectrosc.* **1979**, *13*, 47.
(20) Heatley, F. *Annu. Rep. NMR Spectrosc.* **1986**, *17*, 47.
(21) Jones, A. A.; Stockmayer, W. H. *J. Polym. Sci. Polym. Phys. Ed.* **1977**, *15*, 847.
(22) Hall, C. K.; Helfand, E. *J. Chem. Phys.* **1982**, *77*, 3275. Weber, T. A.; Helfand, E. *J. Phys. Chem.* **1983**, *87*, 2881.
(23) Dejean de la Batie, R.; Laupretre, F.; Monnerie, L. *Macromolecules* **1988**, *21*, 2045.
(24) Valeur, B.; Jarry, J. P.; Geny, F.; Monnerie, L. *J. Polym. Sci. Polym. Phys. Ed.* **1975**, *13*, 667.
(25) Dais, P.; Nedea, M. E.; Morin, F. G.; Marchessault, R. H. *Macromolecules* **1990**, *23*, 3387.
(26) Spyros, A.; Dais, P. *J. Polym. Sci. Polym. Phys. Ed.*, submitted for publication.
(27) Wittebort, R. J.; Szabo, A. *J. Chem. Phys.* **1978**, *69*, 1722.
(28) Rose, M. E. *Elementary Theory of Angular Momentum*; Wiley: New York, 1957.
(29) Woessner, D. E. *J. Chem. Phys.* **1962**, *31*, 1.
(30) Jones, A. A. *J. Polym. Sci. Polym. Phys. Ed.* **1977**, *15*, 863.
(31) Connolly, J. J.; Gordon, E.; Jones, A. A. *Macromolecules* **1984**, *17*, 22.
(32) Gronski, W. *Makromol. Chem.* **1979**, *180*, 119.
(33) Dais, P. *Magn. Reson. Chem.* **1989**, *27*, 61.
(34) Dais, P. *Magn. Reson. Chem.* **1987**, *25*, 141. Levy, G. C.; White, D. M.; Anet, F. A. *J. Magn. Reson.* **1972**, *6*, 453.
(35) Riseman, J.; Kirkwood, J. G. *J. Chem. Phys.* **1949**, *16*, 442.
(36) Denault, J.; Prud'homme, J. *Macromolecules* **1989**, *22*, 1307.
(37) Monnerie, L. *J. Non-Cryst. Solids* **1991**, *131*, 755.
(38) Laupretre, F.; Bokobza, L.; Monnerie, L. *Polymer* **1993**, *34*, 468.
(39) Kramers, H. A. *Physica* **1950**, *7*, 248.
(40) Glowinkowski, S.; Gisser, D. J.; Ediger, M. D. *Macromolecules* **1990**, *23*, 3520.
(41) Dais, P.; Nedea, M. E.; Morin, F. G.; Marchessault, R. H. *Macromolecules* **1989**, *23*, 3520.
(42) Helfand, E. *J. Chem. Phys.* **1971**, *54*, 4651.
(43) Adolf, D. B.; Ediger, M. D. *Macromolecules* **1992**, *25*, 1074.
(44) Spyros, A.; Dais, P.; Heatley, F. *Macromolecules*, in press.
(45) Guillermo, A.; Dupeyre, R.; Cohen-Addad, J. P. *Macromolecules* **1990**, *23*, 1291.
(46) Gisser, D. J.; Glowinkowski, S.; Ediger, M. D. *Macromolecules* **1991**, *24*, 4270.
(47) Cowie, J. M. G.; Ferguson, R. *Polymer* **1987**, *28*, 503.
(48) Heijboer, J.; Baas, J. M. A.; van de Graaf, B.; Hoefnagel, M. A. *Polymer* **1987**, *28*, 509.
(49) Coulter, P.; Windle, A. H. *Macromolecules* **1989**, *22*, 1129.
(50) Spyros, A.; Dais, P.; Marchessault, R. H. *J. Polym. Sci., Polym. Phys. Ed.*, submitted for publication.
(51) Wittebort, R. J.; Szabo, A.; Gurd, R. N. *J. Am. Chem. Soc.* **1980**, *102*, 5723.
(52) Levy, G. C.; Axelson, D. E.; Schwartz, R.; Hockmann, J. *J. Am. Chem. Soc.* **1978**, *100*, 410.
(53) Aspler, J. S.; Guillet, J. E. *Macromolecules* **1979**, *12*, 1082.
(54) Merle-Aubry, L.; Holden, D. A.; Merle, Y.; Guillet, J. E. *Macromolecules* **1980**, *13*, 1138.
(55) Holden, D. A.; Guillet, J. E. *Macromolecules* **1980**, *13*, 289.
(56) Holden, D. A.; Rendal, W. A.; Guillet, J. E. *Ann. N.Y. Acad. Sci.* **1981**, *366*, 11.
(57) Holden, D. A.; Wang, P. Y. K.; Guillet, J. E. *Macromolecules* **1980**, *13*, 295.
(58) De Schryver, F. C.; Collart, P.; Vandendriessche, J.; Goodeweeck, R.; Swinner, A.; van der Auweraer, M. *Acc. Chem. Res.* **1987**, *20*, 159.